Droplets Population Balance in a Rotating Disc Contactor: An Inverse Problem Approach

A. Vikhansky and M. Kraft
Dept. of Chemical Engineering, University of Cambridge, Cambridge CB2 3RA, U.K.

M. Simon, S. Schmidt, and H.-J. Bart
Dept. of Mechanical and Process Engineering, Technical University Kaiserslautern, 67653, Kaiserslautern, Germany

DOI 10.1002/aic.10735
Published online December 16, 2005 in Wiley InterScience (www.interscience.wiley.com).

An inverse problems method is applied to a two-phase liquid–liquid system in a rotating disc contactor (RDC). The dispersed phase is modeled by population balance equations, which are solved by a Monte Carlo method, together with the equations for the parametric derivatives of the solution with respect to the parameters of the model. The best-fitting problem is solved by a gradient search method. Because the inverse problem is ill-posed, the iteration procedure is augmented by an appropriate termination criterion to stabilize the calculations. The parametric derivatives of the solution can be used to quantify the relative importance of different parameters of the model. It is shown that the model's parameters, which are identified on one set of the experimental data, adequately describe the behavior of the system under another unfitted operation condition, that is, the proposed method can be applied to scale-up problems. © 2005 American Institute of Chemical Engineers *AIChE J,* 52: 1441–1450, 2006

Keywords: two-phase systems, sensitivity analysis, inverse problems, Monte Carlo, population balances, weighted particles method

Introduction

The common framework for the description and analysis of two-phase systems consists of mass, momentum, and energy balances, which require some additional closure relationships to make the equations mathematically tractable. A difficulty arises from the relationship between the available experimental data and the information that is needed for an analytical description of multiphase flows. The experimentally accessible quantities such as gas holdup or interphase area characterize the dispersed system as a whole, whereas the mathematical modeling requires more detailed information about single droplet behavior and droplet–droplet interaction. Therefore, an additional mathematical treatment is necessary to extract this information from the measurements, that is, the solution of the inverse problem is a necessary part of a reliable modeling strategy.

Inverse problems for population balances have attracted much attention in recent years.[1-6] The solution of inverse problems is often aided by the self-similar behavior of many practically important dispersed systems.[2,4] In more general cases a mathematical programming procedure has to be applied to find the best fit of the experimental data. Note that inverse problems are highly sensitive to errors in the experimental data.[7] Because the experimental results always contain some noise, a regularization scheme has to be implemented to make the numerical algorithm stable.

In the present study we consider liquid–liquid flow in a pilot-scale rotating disc contactor (RDC).[8] The parameter-fitting problem is solved by a gradient-search algorithm,[9] where a Monte Carlo method is used for the solution of the population balance problem and the calculation of the parametric derivatives of the solution. This approach has several important advantages: (1) a Monte Carlo method can easily be extended

Correspondence concerning this article should be addressed to M. Kraft at mk306@cam.ac.uk.

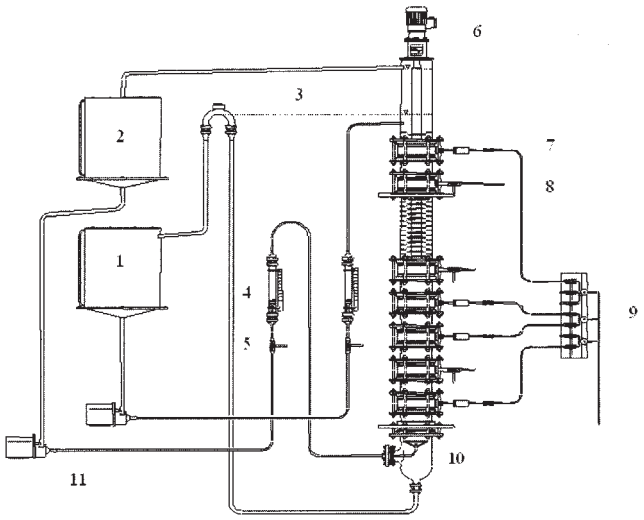

Figure 1. View of the rotating disc contractor.

Legend: 1, water reservoir; 2, organic-phase reservoir; 3, water overflow; 4, flow meter; 5, valve; 6, motor; 7, droplet sampling tube; 8, valve for holdup measurement; 9, control valve system for the droplet size measurement device; 10, distributor; 11, pump.

to a multidimensional case; (2) gradient search is faster than other methods of mathematical programming; (3) an efficient regularization scheme, that is, iterative regularization[10] can be used; and (4) the parametric derivatives indicate which parameters should be identified accurately and which can be postulated approximately because of their weak effect on the simulation results.

Experimental

The view of the RDC[8] is given in Figure 1. The device is 2200 mm high (active length is 1500 mm), its internal diameter is 150 mm, and the diameter of the rotating shaft is $D_s = 54$ mm. The external diameter of the discs and the internal diameter of the baffles are $D_r = 92$ mm and $D_b = 105$ mm, respectively. The extraction system examined is the EFCE water–toluene test system.[11] Before each experiment the continuous water phase and the dispersed toluene phase have been mutually saturated. The angular velocity of the shaft Ω_s varies from 250 to 450 rpm. The continuous phase, which has higher density $\rho_c = 0.998$ g/cm^3 and viscosity $\mu_c = 0.92$ g cm^{-1} s^{-1}, is supplied from above with volume flux $Q_c = 50$–120 L/h, that is, the average downward velocity is <0.18 cm/s, which is several orders of magnitude less than the local velocities encountered in the system.

The dispersed (lighter) phase, with density $\rho_d = 0.856$ g/cm^3, is supplied through the bottom of the column with volume flux $Q_d = 50$–120 L/h. The interphase pressure tension is $\sigma = 36$ g/s^2. For varying operational conditions droplet size distributions and holdup values (volume fraction of the dispersed phase) were measured at different column heights. To measure the droplet size distributions the established method by Pilhofer and Miller[12] was used; each sample contains from 500 to 800 droplets. Samples were taken with a photoelectrical capillary suction probe. The holdup of the dispersed phase was determined locally by the direct sampling method.

Initially, the volume of the droplets is distributed according to an initial volume distribution; as the droplets move through the RDC, the distribution changes as a result of coalescence and breakage. Because of the rotation of the discs the fluid is centrifuged outward in the radial direction and after impinging on the outer wall is reflected inward to form vorticity cells in each compartment.[13] The droplets rise but are trapped by the vorticity in each compartment, thus playing the role of partially mixed reactors.

The power input in one compartment P is given by[8]

$$P = 8.48\mathrm{Re}_r^{-0.4}\Omega_s^3 D_r^5$$

where Re_r is the Reynolds number of the rotor:

$$\mathrm{Re}_r = \frac{\rho_c D_r^2 \Omega_s}{\mu_c}$$

The number density of the droplets of diameter a at time t is $n(t, a)$ and the volume fraction of the droplets of diameter a to $a + da$ is $\phi(t, a)da = \pi a^3/6n(t, a)da$, whereas the total volume fraction of the droplets in a compartment is $\Phi(t) = \int_0^\infty \phi(t, \xi)d\xi$. Then the equation of population balance of droplet size distribution in a compartment reads

$$\frac{\partial \phi(t, a, c)}{\partial t} = B(\phi, c) - D(\phi, c) \tag{1}$$

where B and D represent birth and death of the droplets, respectively. The unknown (generally speaking, vector) parameter c has to be extracted from the experimental data. In the present investigation we assume that the system is in steady state and the RDC is long enough to neglect the inlet/outlet effects. The observations show that, initially, the characteristic size of the droplets decreases as a result of the breakage when the droplets rise, but in the central part of the RDC the breakage and coalescence are mutually balanced. All the measurements presented in this article are done in the 104th compartment (out of 176) of the RDC. Thus we apply to this compartment the periodic boundary conditions, that is, the compartment above and below the given one have the same droplet size distributions.

Two-Phase Hydrodynamics Model: Breakage, Coalescence, and Transport

According to the common view on the fragmentation of bubbles and droplets in turbulent flows, a droplet breaks if the dynamic pressure arising from the turbulence exceeds the pressure arising from the surface tension, whereas the mechanisms that govern the size distribution of the resulting daughter droplets are less clear. The surface pressure of a drop with diameter a is $\tau_s(a) = 6\sigma/a$. The dynamic pressure of the turbulence at the scale of the drop $\tau_s(a)$ is exponentially distributed with parameter

$$\bar{\tau}_t = \frac{1}{2}\rho_c\overline{\Delta u^2(a)} = \frac{1}{2}\beta\rho_c(\varepsilon a)^{2/3}$$

where $\overline{\Delta u^2(a)}$ is the characteristic velocity difference between two points separated by distance a; the constant $\beta = 8.2$ was given by Batchelor[14]; and ε is the mean dissipation rate of the turbulence, which is the power input P divided by the volume of the compartment. The fraction of eddies with a dynamic pressure $> \tau_s(a)$ is

$$\int_{\tau_s(a)}^{\infty} \exp\left(-\frac{\tau}{\bar{\tau}_t}\right) d\frac{\tau}{\bar{\tau}_t} = \exp\left[-\frac{\tau_s(a)}{\bar{\tau}_t}\right] \tag{2}$$

The time that is necessary for breakage can be estimated as the life time of the turbulent vortex with size a:

$$\frac{1}{t_{break}} = \frac{\sqrt{\overline{\Delta u^2(a)}}}{a} = \sqrt{\beta}\,\frac{\varepsilon^{1/3}}{a^{2/3}} \tag{3}$$

Combining Eqs. 2 and 3 yields the following formula for the droplets breakage rate[15]:

$$c_1\sqrt{\beta}\,\frac{\varepsilon^{1/3}}{a^{2/3}} \exp\left(-c_2\,\frac{\sigma}{\beta\rho_c\varepsilon^{2/3}a^{5/3}}\right) \tag{4}$$

where c_1 and c_2 are empirical constants that must be identified.

Although the general mechanisms of droplets breakage in a turbulent flow are known, less information is available about the size distribution of the daughter droplets formed upon breakage. In the present investigation we have assumed that a droplet with volume v breaks into two droplets with volumes v' and $v - v'$, respectively. The volume v' of the daughter droplet is generated as

$$v' = \frac{v}{\pi}\arccos(1 - 2\gamma)$$

where $0 \le \gamma \le 1$ is a uniformly distributed random variable. Note that more sophisticated breakage models, which can be found in the literature (see, for example, Tsouris and Tavlarides[16] and references therein), contain more empirical constants and thus require a greater amount of experimental data to identify them. As shown below, the given experimental data do not allow a unique solution of the inverse problem; thus introduction of additional empirical parameters leads to unnecessary complexity of the mathematical model.

The coalescence rate of two droplets with volumes and diameters v_1, v_2, a_1, and a_2, respectively, was described in Coulaloglou and Tsouris[15] as the product of the collision frequency $h_{1,2}$ and efficiency of the collision $\lambda_{1,2}$. The relations for $h_{1,2}$ and $\lambda_{1,2}$ are

$$h_{1,2} = c_3\,\frac{\varepsilon^{1/3}}{1+\Phi}\,(v_1^{1/3} + v_2^{1/3})^2(v_1^{2/9} + v_2^{2/9})^{1/2}$$

$$\lambda_{1,2} = \exp\left\{-c_4\,\frac{\mu_c\rho_c\varepsilon}{\sigma^2(1+\Phi)^3}\left(\frac{a_1a_2}{a_1+a_2}\right)^2\right\}$$

The residence time of a droplet of size a in the compartment is

$$\tau_{res}(a) = \frac{h_c}{v(a)}$$

where h_c is the height of the compartment and $v(a)$ is the rising velocity. The rising velocity is the sum of the relative velocity of the droplet with respect to the continuous phase $v_r(a)$ and the (downward directed) velocity of the continuous phase v_c:

$$v(a) = v_r(a) + v_c = v_r(a) - \frac{Q_c}{A(1-\Phi)}$$

where A is the cross section of the column.

Different correlations have been proposed to model the rising velocity of the droplets in extraction columns (see, for example, Ghalehchian and Slater[17] and Godfrey and Slater[18] and references therein). The general approach is to relate $v_r(a)$ to the terminal velocity of a single droplet $v_T(a)$:

$$v_r(a) = k_v v_T(a)$$

where k_v is a slowing factor that takes into account the effects of the column's internals and flow structures inside the compartments. Generally speaking, k_v is a function of column geometry, void fraction of the dispersed phase, and the rotation velocity of the shaft. The empirical correlations for k_v available in the literature contain a large number (five to six) of empirical parameters. Our numerical experiments show that the available amount of experimental data does not allow for reliable identification of so many parameters. On the other hand, a much simpler model, that is, constant slowing factor

$$k_v = c_5$$

satisfactorily approximates the experimental results for the whole range of the operational conditions and predicts right volume fraction of the dispersed phase.

The correlation that we used for $v_T(a)$ reads[8]

$$v_T(a) = \frac{a}{4.2}\left(g\,\frac{\rho_c - \rho_d}{\rho_c}\right)^{2/3}\left(\frac{\rho_c}{\mu_c}\right)^{1/3}\left(1 - \frac{\text{Eö}}{6}\right)$$

where Eö is the Eötvös number:

$$\text{Eö} = \frac{ga^2(\rho_c - \rho_d)}{\sigma}$$

Parameter Identification

The purpose of the present work is not only to fit the experimental results, but also to check whether the fitted model can predict the dynamics of the system under other, unfitted conditions. To achieve this task we divided the experiments, with operation conditions presented in Table 1, into two groups. Experiments (a)–(c) with relatively low flow rate of the dispersed phase were used to identify the parameters c_i of the

Table 1. Operational Conditions of RDC

Experiment	Ω_s (rpm)	Q_d (L/h)	Q_c (L/h)
(a)	300	56	100
(b)	350	56	100
(c)	450	56	100
(d)	250	120	100
(e)	300	112	50
(f)	350	120	100

model and then the fitted model was applied to scale-up of the system, that is, to predict the outcome of the experiments (d)–(f) as shown in Figure 2, which have a higher flow rate. Note that in the steady state, multiplication of the breakage and collision preexponential factors c_1 and c_2 by the same constant does not change the solution. Thus in the present work we assume that $c_1 = 2.0 \times 10^{-2}$ (a value similar to that recommended in the literature) and identify only four parameters $c_2, \ldots, c_5$.

In each experiment the dispersed phase volume fraction and number size distribution function are measured. Because the available experimental data are quite noisy, we use them to calculate several first *mass*-averaged moments, which are less affected by the experimental error. The expression for the jth moment obtained in the ith experiment reads

$$D_{ij} = \int \phi_i(a) a^j da = \frac{\pi}{6} \int n_i(a) a^{(j+3)} da \qquad j = 0, \ldots, 3$$

Then we solve an identification procedure, that is, look for the set of parameters $\vec{c^*} = (c_2^*, \ldots, c_2^*)$ that minimizes the residual between the predicted and the experimental results:

$$\Theta = \frac{1}{2} \sum_{i=1,j=0}^{3} \varrho_j \left(\frac{D_{ij}(\vec{c}) - D_{ij}^{exp}}{D_{ij}^{exp}} \right)^2 \tag{5}$$

where $\varrho_j = 1/2^j$ is an empirical weighting factor, that is, holdup has to be fitted more accurately than the dispersion of the diameter.

We solve Eq. 5 by a quasi-Newtonian algorithm, where a Monte Carlo method is used for the solution of Eq. 1 and the calculation of the gradients $\partial\phi/\partial c$. The details of the algorithm[9] are given in the Appendix. As soon as the parametric deriva-

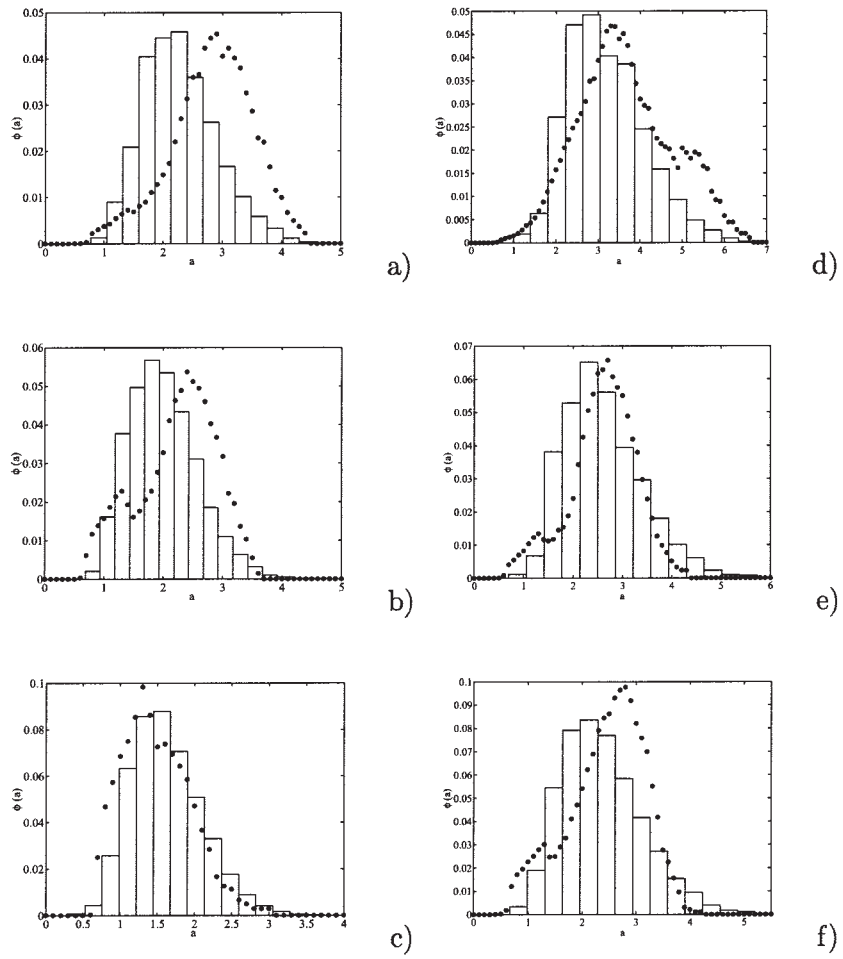

Figure 2. Fitted (a–c, left column) and unfitted (d–f, right column) numerical (histograms) and experimental (points) volume density functions $\phi(a)$ (mm^{-1}) as a function of the diameter.

The operational conditions are given in Table 1.

Table 2. Identified Parameters and Residuals

Iteration	c_2	c_3	c_4	c_5	Θ	$\|\nabla\Theta\|$
0	10.0	2.00e-2	1.00e3	0.300	1.85e-1	2.93e-1
1	6.87	1.43e-2	1.16e3	0.260	8.14e-2	2.18e-1
2	8.08	1.29e-2	1.29e3	0.268	6.24e-2	3.40e-2
3	9.10	1.17e-2	1.63e3	0.264	6.12e-2	3.29e-2

tives are known, an efficient quasi-Newtonian method can be applied to the minimization of the residual Eq. 5. We use the following minimization algorithm; at each iteration $\vec{c}$ is represented as $\vec{c} + \Delta\vec{c}$. Because the parameters c_i have different orders of magnitude, we rescale the increments of the parameters as $\Delta c_i = c_i\beta_i$, where $\beta \cong 1$. Then we expand the moments D_{ij} as $D_{ij}(\vec{c}) = D_{ij}(\vec{c}) + \beta_l c_l \partial_{c_l} D_i(\vec{c})$. Substitution of this formula into Eq. 5 and differentiation with respect to $\vec{\beta}$ yields the following system of linear algebraic equations with respect to the relative increment $\vec{\beta}$:

$$A\vec{\beta} = \vec{b} \tag{6}$$

where

$$a_{lm} = \sum_{i=1,j=0}^{3} \varrho_j \left(\frac{\partial D_{ij}}{\partial c_l} \frac{\partial D_{ij}}{\partial c_m} \right) \frac{c_l c_m}{(D_{ij}^{exp})^2} \tag{7}$$

and

$$b_l = \sum_{i=1,j=0}^{3} \varrho_j c_l \frac{D_{ij}^{exp} - D_{ij}(\vec{c})}{(D_{ij}^{exp})^2} \frac{\partial D_{ij}}{\partial c_l} \tag{8}$$

One can see that the vector $\vec{b}$ is nothing else but the gradient of the residual Θ with respect to β.

Note, that the matrix A is badly scaled, and thus we regularize Eq. 6 as

$$(sE + A)\vec{\beta} = \vec{b} \tag{9}$$

where s is a parameter of regularization and E is a unit matrix. The error arising from the regularization $\varepsilon = (A\vec{\beta} - \vec{b})^2$, plotted as a function of $1/s$, is low for high s and has a characteristic bend for some value of s. The region of the bend gives a good compromise between the stability and the precision of the computations. If the parameter of regularization s is very high, the above-described method becomes a gradient search method with fixed step.

The difference $(D_{ij}^{exp} - D_{ij})$ in Eq. 8 contains two types of error. One is the systematic error because the model is approximate and cannot reproduce the experimental results exactly. The second error arises from the unavoidable experimental noise that is very strong in every dispersed system and manifests itself in the apparent bimodality of the droplet size distribution. Because we use a Monte Carlo method for the solution of Eq. 1, the computed moments D_{ij} also contain some error. Initially, when the systematic error is larger than the statistical error, the direction of the steepest descend $\vec{b} = \nabla\Theta$ is insensitive to the random noise. Therefore, during the first few iterations of the minimization algorithm the identified parameters approach the exact values, that is, those values that they would have in the "no noise" case. As the residual decreases, the random component has a higher relative contribution to Eq. 8. Because the random components of D_{ij}^{exp} mutually cancel during the summation over i and j, the gradient $\nabla\Theta$ becomes very small. Thus, the identified parameters start to recede from the exact ones, whereas the residual does not decrease significantly. At this point the calculations have to be terminated to avoid instability.[10]

The results of the calculations, presented in Table 2, illustrate this process. During the first two iterations, the residual decreases quickly, whereas at the third iteration the gradient $\nabla\Theta$ sharply decreases and the significant change of the parameters c_i does not improve the solution. Therefore, we can identify the second iteration as the beginning of the instability and terminate the iterations here.

The calculated and measured droplets size distributions are presented in Figure 2. As we can see, the results of the computations approximate both the fitted and the unfitted experimental data with satisfactory precision. Although the unfitted results for conditions (d)–(f) seem to agree better with the experimental data than the fitted ones, they do not approximate the experimental results in the best way. The fitted results shifted both left and right with respect to the corresponding experimental results; thus, better fitting of these results within frameworks of the given model is impossible. The unfitted results are shifted right and the discrepancy between the measured and the calculated results can be reduced further.

To quantify the difference between the experimental and the numerical results we calculated the following characteristics of the dispersed system, that is, the volume fraction of the droplets Φ, their mass-mean diameter

Table 3. Comparison of Experimental and Numerical Results

Experiment	Φ_{num}	Φ_{exp}	ε_Φ (%)	$d_{m_{num}}$	$d_{m_{exp}}$	ε_{d_m} (%)	$d_{s_{num}}$	$d_{s_{exp}}$	ε_{d_s} (%)
(a)	0.0709	0.072	−1.5	2.28	2.77	−18	2.11	2.60	−19
(b)	0.0824	0.0787	5.0	2.00	2.18	−8.3	1.84	1.97	−6.6
(c)	0.104	0.105	−0.95	1.62	1.44	13	1.48	1.37	8.0
(d)	0.111	0.116	−4.3	3.20	3.60	−11	2.95	3.26	−9.5
(e)	0.118	0.0956	23.0	2.60	2.55	2.0	2.37	2.50	−5.2
(f)	0.154	0.158	−2.5	2.37	2.37	−1.3	2.15	2.16	−0.46

Table 4. Sensitivities of the Volume Fraction of the Dispersed Phase Φ, with Respect to the Corresponding Parameters

Experiment	c_1	c_2	c_3	c_4	c_5
(a)	0.1655	−0.3814	−0.1661	0.0353	−0.9668
(b)	0.2011	−0.4602	−0.2063	0.0472	−0.9381
(c)	0.2133	−0.4230	−0.2387	0.0681	−0.9638
(d)	0.1622	−0.3020	−0.1533	0.0368	−0.9675
(e)	0.1951	−0.3790	−0.2052	0.0516	−0.8884
(f)	0.2418	−0.4338	−0.2354	0.0665	−0.9338

$$d_m = \Phi^{-1} \int \phi(a) da$$

and the Sauter mean diameter

$$d_s = \frac{\int n(a) a^3 da}{\int n(a) a^2 da}$$

which are presented in Table 3. The relative difference ε_ϑ between the experimental and the numerical values of a feature ϑ is

$$\varepsilon_\vartheta = \frac{\vartheta_{num} - \vartheta_{exp}}{\vartheta_{exp}}$$

The relative error does not exceed 20%; the only exception is experiment (e). As one can see, the experimentally obtained volume density functions contain some noise. From general considerations we would expect that a higher agitation rate increases the volume fraction of the dispersed phase [one can compare experiments (a)–(c)], whereas the value of Φ registered in experiment (e) is lower than that in (d), which corresponds to the lower angular velocity of the shaft. Thus, we assume that part of the error arises from the experimental noise, which is unavoidable in two-phase systems. In spite of the relatively high discrepancy between the experimental and the numerical results, it is still lower than the difference between different experimental conditions, and thus the model correctly predicts the main trend of the system.

Sensitivity Analysis

It is obvious that different empirical parameters have different effects on the solution of Eq. 5. Those parameters that have a weak effect on the output of the computations cannot be identified with reasonable precision. On the other hand, these parameters do not have to be known accurately. The sensitivity analysis gives an opportunity to identify both important and unimportant parameters and their combinations. To proceed further let us expand the residual Θ in the vicinity of the optimal set of parameters c_i^* into a Taylor series:

$$\Theta(\vec{c}) \approx \Theta(\vec{c}^*) + \frac{1}{2} (\vec{c} - \vec{c}^*)^T A (\vec{c} - \vec{c}^*)$$

The matrix U of eigenvectors $\vec{u}_i$ and the vector of corresponding eigenvalues λ_i of the matrix A are

$$U = \begin{pmatrix} 0.0577 & -0.7862 & 0.6138 & -0.0433 \\ 0.0448 & -0.6015 & -0.7570 & 0.2513 \\ -0.0035 & 0.1215 & 0.2242 & 0.9669 \\ 0.9973 & 0.0730 & -0.0007 & -0.0053 \end{pmatrix} \quad (10)$$

and

$$\vec{\lambda}^T = (9.68 \quad 1.65 \quad 9.89\text{e-}3 \quad 3.79\text{e-}4) \quad (11)$$

respectively. If we denote the uncertainty of the residual as $\Delta\Phi$, the uncertainty of the identified parameters in the direction of the eigenvector $\vec{u}_i$ can be estimated as $\Delta\vec{c} \approx (\Delta\Theta/\lambda)^{1/2}\vec{u}_i$. As follows from Table 2, $\Delta\Theta$ can be estimated as $\Delta\Theta \approx 10^{-2}$ and $\Delta\vec{c}$ along the third and the fourth eigenvectors is about 100 and 500%, respectively. The third and fourth columns of matrix U show that, although the slowing factor $k_v = c_5$ can be identified with reasonable precision, simultaneous increase/decrease of collision and coalescence rates or, alternatively, increase/decrease of the preexponential factor c_3 and the exponential coefficient c_4 do not significantly change the results of the computations.

To quantify the effect of different parameters on the solution of Eq. 5 we define the coefficient of sensitivity $S_{c_i}^{\vartheta}$ of a feature ϑ to the coefficient c_i as the ratio of the relative change of ϑ to the relative change of c_i:

Table 5. Sensitivities of Mass-Mean Diameters d_m, with Respect to the Corresponding Parameters

Experiment	c_1	c_2	c_3	c_4	c_5
(a)	−0.1580	0.3629	0.1657	−0.0356	−0.2063
(b)	−0.1833	0.4040	0.1971	−0.0469	−0.2259
(c)	−0.2020	0.4279	0.1958	−0.0552	−0.2534
(d)	−0.1870	0.3331	0.1779	−0.0438	−0.2054
(e)	−0.2368	0.4431	0.2164	−0.0568	−0.1992
(f)	−0.2230	0.3902	0.2171	−0.0617	−0.2604

Table 6. Sensitivities of Sauter Mean Diameters d_s, with Respect to the Corresponding Parameters

Experiment	c_1	c_2	c_3	c_4	c_5
(a)	2.0210	−4.5994	−2.0253	0.4342	−12.8457
(b)	2.0745	−4.7045	−2.1192	0.4896	−10.6512
(c)	1.6482	−3.1708	−1.8679	0.5426	−8.4998
(d)	1.1224	−2.0520	−1.0725	0.2612	−7.9546
(e)	1.2465	−2.3719	−1.3462	0.3435	−6.8062
(f)	1.1236	−1.9540	−1.0990	0.3193	−5.3549

$$S_{c_i}^{\vartheta} = \frac{\Delta \ln \vartheta}{\Delta \ln c_i}$$

The sensitivity coefficients for the volume fraction of the dispersed phase, mass-mean diameter, and Sauter mean diameter are given in Tables 4–6. The signs of the computed sensitivity coefficients are intuitively clear: breakage decreases the mean diameter of the droplets and increases the interphase area. Because smaller droplets have lower terminal velocities, intensive breakage increases the volume fraction of the dispersed phase. The effect of coalescence is opposite to the effect of breakage. One can also see that the exponential coefficient c_4 has a significantly lesser effect than that of other parameters of the model and this coefficient is not identified with high precision.

Conclusions

A Monte Carlo method was applied to a droplet's population balance in two-phase liquid–liquid flow. The method allows for the calculation of the derivatives of the solution with respect to the empirical coefficients of the model. As soon as the parametric derivatives are known, an efficient gradient search method can be used to minimize the difference between the observed and the numerical results, that is, the unknown empirical parameters of the model can be extracted from the available experimental data. Iterative regularization[10] was used to stabilize the solution of the inverse problem. Only a few iterations of the gradient algorithm are required to identify the unknown coefficients. The coefficients identified on the basis of one set of experimental data can be used to predict the behavior of the system under different operation conditions. The proposed methods also provide information about sensitivity of the solution to the parameters of the model; this information can be used to decide which parameters have to be identified with high precision. On the other hand, this method can be used for an experiment design as follows. When some of the parameters are identified and the model has a reasonable agreement with the experimental data, one can calculate the sensitivities of the solution to the rest of the parameters under other experimental conditions and detect which experiments have to be done to identify these parameters.

Acknowledgments

This work has been supported by the EPSRC (Grant GR/R85662/01) under the title "Mathematical and Numerical Analysis of Coagulation–Diffusion Processes in Chemical Engineering."

Literature Cited

1. Colella D, Vinci D, Bagatin R, Masi M, Bakr EA. A study on coalescence and breakage mechanisms in three different bubble columns. *Chem Eng Sci.* 1999;54:4767-4777.
2. Hounslow MJ, Ni X. Population balance modelling of droplet coalescence and break-up in an oscillatory baffled reactor. *Chem Eng Sci.* 2004;59:819-828.
3. Ni X, Mignard D, Saye B, Johnstone JC, Pereira N. On the evaluation of droplet breakage and coalescence rates in oscillatory baffled reactor. *Chem Eng Sci.* 2002;57:2101-2114.
4. Ramkrishna D. *Population Balances*. San Diego, CA: Academic Press; 2000.
5. Ribeiro CP Jr, Lage PLC. Population balance modeling of bubble size distributions in a direct-contact evaporator using a sparger model. *Chem Eng Sci.* 2004;59:2363-2377.
6. Simon M, Schmidt SA, Bart H-J. The droplet population balance model—Estimation of breakage and coalescence. *Chem Eng Technol.* 2003;26:745-750.
7. Tikhonov AN, Arsenin VY. *Solution of Ill-Posed Problems*. Palm Beach, FL: VH Winston & Son; 1977.
8. Modes G. *Grundsätzliche Studie zur Populationsdynamik einer Extraktionskolonne auf Basis von Einzeltropfenuntersuchungen*. PhD Thesis. Kaiserslautern, Germany: Universität Kaiserslautern; 1999.
9. Vikhansky A, Kraft M. A Monte Carlo methods for identification and sensitivity analysis of coagulation processes. *J Comput Phys.* 2004; 200:50-59.
10. Alifanov OM, Artyukhin EA, Rumyantsev SV. *Extreme Methods for Solving Ill-Posed Problems with Applications to Inverse Problems*. New York, NY: Begell House; 1995.
11. Misek T, Berger R, Schröter J. *European Federation of Chemical Engineering: Standard Test Systems for Liquid Extraction*. Rugby, UK: The Institution of Chemical Engineers; 1985.
12. Pilhofer T, Miller HD. Photoelektrische messmethode zur bestimmung der tropfengrenverteilung mitteldisperser tropfen in einem nichtmischbaren flssigen zweistoffsystem. *Chem-Ing-Tech.* 1972;44:295-300.
13. Vikhansky A, Kraft M. Modeling of RDC using a combined CFD-population balance approach. *Chem Eng Sci.* 2004;59:2597-2606.
14. Batchelor GK. *The Theory of Homogeneous Turbulence*. Cambridge, UK: Cambridge Univ. Press; 1956.
15. Coulaloglou CA, Tsouris C. Description of interaction processes in agitated liquid–liquid dispersions. *Chem Eng Sci.* 1977;32:1289-1297.
16. Tsouris C, Tavlarides LL. Breakage and coalescence model for drops in turbulent dispersions. *AIChE J.* 1994;40:395-406.
17. Ghalehchian JS, Slater MJ. A possible approach to improving rotating disc contactor design accounting for drop breakage and mass transfer with contamination. *Chem Eng J.* 1999;75:131-144.
18. Godfrey JC, Slater MJ. Slip velocity relationships for liquid–liquid extraction columns. *Trans IChemE.* 1991;69:130-141.
19. Eibeck A, Wagner W. Stochastic particle approximation for Smoluchovski's coagulation equation. *Ann Appl Probab.* 2001;11:1137-1165.
20. Goodson M, Kraft M. Simulation of coalescence and breakage: An assessment of two stochastic methods suitable for simulating liquid–liquid extraction. *Chem Eng Sci.* 2004;59:3865-3881.
21. Ramkrishna D, Sathyagal A, Narishman G. Analysis of dispersed-phase systems: Fresh perspective. *AIChE J.* 1995;41:35-44.
22. Rjasanow S, Schreiber T, Wagner W. Reduction of number of particles in the stochastic weighted method for the Boltzmann equation. *J Comput Phys.* 1998;145:382-405.

A Calculation of Parametric Derivatives of the Solution of the Population Balance Equation

To illustrate the method for calculations of parametric derivatives of the solution of the population balance equation,

consider for simplicity the space-homogeneous Smoluchowski coagulation equation

$$\frac{\partial n(t, x; \lambda)}{\partial t} = \frac{1}{2}\int_0^x K(x - x', x'; \lambda) n(t, x - x'; \lambda)\, n(t, x'; \lambda) dx' - \int_0^\infty K(x, x'; \lambda) n(t, x; \lambda)\, n(t, x'; \lambda) dx' \quad \text{(A1)}$$

where $n(t, x; \lambda)$ is the number density of particles that have mass x at time t. The probability that two particles with masses x and x', respectively, coalesce during a small time interval dt is $K(x, x'; \lambda)dt$, where λ is a parameter. To proceed further let us reformulate Eq. A1 in terms of mass density. The advantages of this formulation are discussed in Eibeck and Wagner[19] and Goodson and Kraft[20]; note also, that particle mass distributions are encountered in technological applications more frequently than number distributions.[4,21] The mass density of the particles that have mass x at a time t is $m(t, x) = xn(t, x)$. The total mass of the system is $M = \int m dx$. To rewrite the coagulation Eq. A1 in terms of mass density, we express $n(t, x)$ as $m(t, x)/x$, substitute it into Eq. A1 and multiply the equation by x. Note, that if $K(x, x') = 0$ for $x \le 0$ or $x' \le 0$, the limits of integration in Eq. A1 can be extended from $-\infty$ to ∞. After some algebra we obtain[4,19]

$$\frac{\partial m(t, x; \lambda)}{\partial t} = \int \frac{K(x - x', x'; \lambda)}{x'} m(t, x - x'; \lambda)\, m(t, x'; \lambda) dx' - \int \frac{K(x, x'; \lambda)}{x'} m(t, x; \lambda) m(t, x'; \lambda) dx' \quad \text{(A2)}$$

The factor 1/2 before the first integral in Eq. A2 disappears because coagulation reduces the number of particles but does not affect their mass.

Consider a stochastic particle system

$$x_1(t), \ldots, x_N(t)$$

which approximates the mass density function $m(t, x)$ as

$$m(t, x) \approx \sum_{n=1}^{N} w_n \delta[x - x_n(t)] \quad \text{(A3)}$$

that is, each particle in the above N-particle system represents a group of identical physical particles with size x_n. The total mass of the nth group is w_n and the number of particles in the group is w_n/x_n. Because the probability that during a small time interval dt the kth particle will coagulate with one particle from the lth group is $K(x_k, x_l; \lambda)dt$, the probability that the kth particle will coagulate with any of the lth particles is

$$\pi_{kl}(\lambda)dt = \frac{K(x_k, x_l; \lambda) w_l}{x_l} dt$$

Thus, the coagulation rate of the kth particle is given by the summation of the above formula over l. The formula for the total collision rate reads

$$\sum_{\alpha=1,\beta=1}^{N} \pi_{\alpha\beta}(\lambda) \quad \text{(A4)}$$

and the collision pair is chosen with the relative probability

$$\frac{\pi_{kl}(\lambda)}{\sum_{\alpha=1,\beta=1}^{N} \pi_{\alpha\beta}(\lambda)} \quad \text{(A5)}$$

In the present investigation we use the acceptance–rejection technique similar to that used in Eibeck and Wagner.[19] Let us consider a majorant kernel and majorant weights satisfying

$$K(x_k, x_l; \lambda) \le \hat{K}(x_k, x_l) \qquad w_l \le \hat{w}_l \qquad \pi_{kl}(\lambda) \le \hat{\pi}_{kl} = \hat{K}(x_k, x_l)\hat{w}_l$$

The corresponding stochastic algorithm reads:

(1) Generate an exponentially distributed time increment τ with parameter

$$\sum_{\alpha=1,\beta=1}^{N} \hat{\pi}_{\alpha\beta} \quad \text{(A6)}$$

(2) Choose a pair (k, l) to collide according to the distribution

$$\frac{\hat{\pi}_{kl}}{\sum_{\alpha=1,\beta=1}^{N} \hat{\pi}_{\alpha\beta}} \quad \text{(A7)}$$

(3) Accept the coagulation with probability

$$\frac{\pi_{kl}(\lambda)}{\hat{\pi}_{kl}} \quad \text{(A8)}$$

that is, x_k is replaced by $x_k + x_l$;

(4) or reject the coagulation and perform a *fictitious* jump that does not change the size of the colliding particles with probability

$$1 - \frac{\pi_{kl}(\lambda)}{\hat{\pi}_{kl}} \quad \text{(A9)}$$

Notably, the number of particles in this algorithm does not change during the calculations. The particle ensemble at time t is an approximation of the mass density function $m(t, x)$.

Now, consider a functional of the solution of Eq. A2:

$$H(t, m; \lambda) = \int m(t, x; \lambda) h(x) dx$$

where $h(x)$ is an integrable function of x. Substitution of Eq. A3 into the above equation gives a Monte Carlo estimate of the functional H that is averaged over the N-particle ensemble:

$$H(t, m; \lambda) \approx \sum_{n=1}^{N} w_n h[x_n(t)] \tag{A10}$$

Let us consider the following formula:

$$H(t, m; \lambda + \Delta\lambda) \approx \sum_{n=1}^{N} w_n (1 + \Delta\lambda W_n) h[x_n(t)] \tag{A11}$$

Comparison with Eq. A10 reveals that

$$\frac{\partial H(t, m; \lambda)}{\partial \lambda} \approx \sum_{n=1}^{N} w_n W_n h[x_n(t)] \tag{A12}$$

and

$$\frac{\partial m(t, x; \lambda)}{\partial \lambda} \approx \sum_{n=1}^{N} w_n W_n \delta[x - x_n(t)]. \tag{A13}$$

The above formula can be interpreted as a parametric derivative (in a weak sense) of the solution of Eq. A2, and $W_n = (\partial_\lambda w_n)/w_n = \partial_\lambda \ln w_n$.

We will refer to a system with weights $w_n(1 + \Delta\lambda W_n)$, kernel $K(x_k, x_l; \lambda + \Delta\lambda)$, and

$$\pi_{kl}(\lambda + \Delta\lambda) = \frac{K(x_k, x_l; \lambda + \Delta\lambda) w_n (1 + \Delta\lambda W_n)}{x_l}$$

as the "*disturbed*" system, whereas the original system is referred to as an "*undisturbed*" system. The time evolution of the disturbed system is as follows. Given that Eqs. A6 and A7 do not depend on λ, the only difference between the disturbed and undisturbed systems is at the acceptance–rejection step. The coagulation is accepted with probability

$$\frac{\pi_{kl}(\lambda + \Delta\lambda)}{\hat{\pi}_{kl}}, \tag{A14}$$

or rejected with probability

$$1 - \frac{\pi_{kl}(\lambda + \Delta\lambda)}{\hat{\pi}_{kl}}. \tag{A15}$$

After this step the average contribution of the kth particle to the functional Eq. A11 reads

$$h(x_k + x_l) w_k (1 + \Delta\lambda W_k) \times \frac{\pi_{kl}(\lambda + \Delta\lambda)}{\hat{\pi}_{kl}} + h(x_k) w_k \times (1 + \Delta\lambda W_k) \times \left[1 - \frac{\pi_{kl}(\lambda + \Delta\lambda)}{\hat{\pi}_{kl}}\right].$$

Expanding the above formula with respect to $\Delta\lambda$ and keeping the terms up to $O(\Delta\lambda)$ one obtains the average contribution of the kth particle to the functional H:

$$h(x_k + x_l) w_k [1 + \Delta\lambda(W_k + \partial_\lambda \ln \pi)] \times \frac{\pi_{kl}(\lambda)}{\hat{\pi}_{kl}} + h(x_k) w_k \times \left[1 + \Delta\lambda\left(W_k - \pi \frac{\partial_\lambda \ln \pi}{\hat{\pi} - \pi}\right)\right] \times \left[1 - \frac{\pi_{kl}(\lambda)}{\hat{\pi}_{kl}}\right].$$

Comparison of the above formula with Eqs. A8 and A9 shows that the probabilities of acceptance and rejection in the disturbed system can be the same as those in the undisturbed system (that is, initially all factors $W_k = 0$); the system evolves along the trajectory of the undisturbed system, whereas at each step (fictitious and nonfictitious) the factors W_k have to be recalculated as

$$W_k = W_k + \partial_\lambda \ln(\pi_{kl}) = W_k + \partial_\lambda \ln(K) + W_l \tag{A16}$$

if the coagulation is accepted, or as

$$W_k = W_k - \pi_{kl} \frac{\partial_\lambda \ln \pi_{kl}}{\hat{\pi}_{kl} - \pi_{kl}} = W_k - w_l K \frac{\partial_\lambda \ln(K) + W_l}{\hat{w}_l \hat{K} - w_l K} \tag{A17}$$

if the coagulation is rejected. If the particle undergoes breakage or any other process that (unlike coalescence) involves only one particle, similar considerations yield the following formula for recalculation of W_k. Let $g(\lambda)$ be the breakage rate and $\hat{g} \geq g(\lambda)$ be a majorant. Then we accept the breakage with the probability $g(\lambda)/\hat{g}$ and recalculate the factor W_k as

$$W_k = W_k + \partial_\lambda \ln[g(\lambda)], \tag{A18}$$

or reject it with the probability $1 - g(\lambda)/\hat{g}$ and recalculate the factor W_k as

$$W_k = W_k + \partial_\lambda \ln[1 - g(\lambda)/\hat{g}]. \tag{A19}$$

This method for sensitivity analysis of population balance equations has been tested in our previous work[9] and it was shown that the estimation of the parametric derivatives based on Eqs. A16 and A17 has high dispersion. To understand the origin of this dispersion it is sufficient to note that two identical particles with factors W and $-W$, respectively, give zero contribution to the parametric derivative for any (high) value of W. The numerical experiments show that the factors W can grow infinitely, which leads to unbounded dispersion of the calculated derivatives. To reduce the dispersion we used a weighted-particles algorithm that creates one additional particle after each collision, after which we used a clustering method[22] to reduce the number of particles.

In the present investigation we use an alternative method that does not require the time-consuming clustering procedure. Assume that we do not need to calculate the parametric derivative of the solution $\partial m(x)/\partial\lambda$ but only derivatives of some first moments of the particle size distribution: total mass, mean diameter, and so forth. Define a set of functions $h_0(x)$, $h_1(x)$, . . . , $h_K(x)$ [such as $h_k(x) = x^{k/3}$]. Substitution of these functions into Eq. A12 yields a system of linear equations with respect to W_n:

$$\sum_{n=1}^{N} \{h_k(x_n)w_n\}W_n = \frac{\partial H_k(m;\,\lambda)}{\partial\lambda}\,. \tag{A20}$$

The solution of the problem

$$\min_{W_n} \frac{1}{2}\sum_{n=1}^{N} W_n^2 \tag{A21}$$

that satisfies Eq. A20 does not change the parametric derivatives $\partial H_k/\partial\lambda$ of the first K moments and reduces the scatter of the factors W_n.

Finally, the algorithm for calculation of the parametric derivatives is as follows. We simulate the coagulation process according to Eqs. A6–A9 and recalculate W_n according to Eqs. A16–A19. When the scatter of the factors W_n becomes too high we solve the problem A20 and A21. Because we do not need an exact minimum of Eq. A21, two to four iterations of a projective gradient method are enough to stabilize the computations. Note that this procedure is not time-consuming and the required CPU time scales almost linearly with the number of the preserved moments K. The computational experiments with K spans from 6 to 24 give very close results. All the results presented in this work were obtained with $K = 16$.

Manuscript received Feb. 24, 2005, revision received Aug. 1, 2005, and final revision received Oct. 20, 2005.